The results presented here are a first attempt at investigating expected global trends in surface UVR in the context of cloud variability, and we now give several cautionary notes. First, the cloud reflectance dataset (ERBE) has a duration of only five years, and could therefore provide a first-order estimate of interannual variability, but not any estimate of possible trends in the global cloud cover itself. Second, the global trends in ozone used here[2] were derived from TOMS data over the period 1978–91. There have been some pronounced ozone depletion events during the early 1990s[15], but on the other hand, ozone depletions are expected to recover during the first half of the next century as a result of the 1987 Montreal Protocol. Certainly this type of study should be repeated periodically, as the TOMS or similar ozone time series becomes longer and the regional ozone trends are revised accordingly. Third, in this study tropospheric ozone is held constant. Tropospheric ozone can provide a noticeable absorption of UV-B (280–315 nm) flux in the presence of cloud scattering[16], and for regions where tropospheric ozone abundance may be increasing (for example, industrialized regions), the elapsed times reported here might best be considered as lower limits. Fourth, satellite investigations of this kind should not be taken as a substitute for deploying a global ground-based UVR monitoring network using spectral radiometric equipment. Fifth, we have examined the significance of UVR trends with respect to cloud variability because the issue of cloud opacity has hitherto been considered an unknown quantity on a global basis. We have not discussed detection of UVR trends with respect to variability in ozone; this is beyond the scope of this study and is best addressed by ground-based spectral UVR measurements[17–19]. There are some reasons for being concerned about peak (cloud-free) rather than climatological UVR exposure[20,21] (for example, the effects of recreational sun exposure in humans), and in the cloud-free case our threshold for biological significance is reached immediately. Last, we have discussed here only the elapsed time from the onset of ozone depletion to when a trend in a given biological UVR dose rate would just begin to exceed the bounds under which ecosystems have adapted, as defined by interannual variability in cloud opacity. The ecological significance of this should be determined by the workers in the area of photobiology. □

Received 8 May; accepted 21 September 1995.

1. Bojkov, R., Bishop, L., Hill, W. J., Reinsel, G. C. & Tiao, G. C. *J. geophys. Res.* **95,** 9785–9807 (1990).
2. Niu, X., Frederick, J. E., Stein, M. L. & Tiao, G. C. *J. geophys. Res.* **97,** 14661–14669 (1992).
3. Stolarski, R. S., Bloomfield, P. & McPeters, R. D. *Geophs. Res. Lett.* **18,** 1015–1018 (1991).
4. Ramanathan, V. *et al. Science* **243,** 57–63 (1989).
5. Joseph, J. H., Wiscombe, W. J. & Weinman, J. A. *J. atmos. Sci.* **33,** 2453–2459 (1976).
6. Li, Z. & Garand, L. *J. geophys. Res.* **99,** 8335–8350 (1994).
7. Briegleb, B. P. *J. geophys. Res.* **97,** 7603–7612 (1992).
8. Wittmeyer, I. L. & Vonder Haar, T. H. *J. Clim.* **7,** 326–333 (1994).
9. Lubin, D., Ricchiazzi, P., Gautier, C. & Whritner, R. H. in *Ultraviolet Radiation in Antarctica: Measurements and Biological Effects* (eds Weiler, S. & Penhale, P.) 53–81 (Antarctic Res. Ser. Vol. 62, Am. Geophys. Union, Washington DC, 1994).
10. Madronich, S. in *Environmental UV Photobiology* (eds Young, A. R., Björn, L. O., Moan, J. & Nultsch, W.) 1–39 (Plenum, New York, 1993).
11. Cole, C. A., Forbes, D. & Davies, R. E. *Photochem. Photobiol.* **43,** 275–284 (1986).
12. Quaite, F. E., Sutherland, B. M. & Sutherland, J. C. *Nature* **358,** 576–578 (1992).
13. Frederick, J. E. & Lubin, D. *J. geophys. Res.* **93,** 3825–3832 (1988).
14. Eck, T. F., Bhartia, P. K. & Kerr, J. B. *Geophys. Res. Lett.* **22,** 611–614 (1995).
15. Gleason, J. F. *et al. Science* **260,** 523–526 (1993).
16. Brühl, C. & Crutzen, P. J. *Geophys. Res. Lett.* **16,** 703–706 (1989).
17. Lubin, D. *et al. J. geophys. Res.* **97,** 7817–7828 (1992).
18. Stamnes, K., Slusser, J., Bowen, M., Booth, C. R. & Lucas, T. *Geophys. Res. Lett.* **17,** 2181–2184 (1990).
19. Seckmeyer, G. *et al. Geophys. Res. Lett.* **22,** 1889–1892 (1995).
20. Madronich, S. *Geophys. Res. Lett.* **19,** 37–40 (1992).
21. Blumthaler, M. & Ambach, W. *Science* **248,** 206–208 (1990).
22. Liou, K. N. *Radiation and Cloud Processes in the Atmosphere* 305–307 (Oxford Univ. Press, 1992).
23. Pilewskie, P. & Valero, F. P. J. *Science* **267,** 1626–1629 (1995).
24. Li, Z., Barker, H. W. & Moreau, L. *Nature* **376,** 486–490 (1995).
25. Ramanathan, V. & Collins, W. *Nature* **351,** 27–32 (1991).

ACKNOWLEDGEMENTS. We thank W. Collins and W. Hunter of the Center for Clouds, Chemistry and Climate for facilitating access to the ERBE data. This work was supported by NASA.

The internal structure of an active sea-floor massive sulphide deposit

Susan E. Humphris[1], P. M. Herzig[2], D. J. Miller[3], J. C. Alt[4], K. Becker[5], D. Brown[6], G. Brügmann[7], H. Chiba[8], Y. Fouquet[9], J. B. Gemmell[10], G. Guerin[11], M. D. Hannington[12], N. G. Holm[13], J. J. Honnorez[14], G. J. Iturrino[5], R. Knott[15], R. Ludwig[16], K. Nakamura[17], S. Petersen[2], A-L. Reysenbach[18], P. A. Rona[19], S. Smith[20], A. A. Sturz[21], M. K. Tivey[22] & X. Zhao[23]

THE hydrothermal circulation of sea water through permeable ocean crust results in rock–water interactions that lead to the formation of massive sulphide deposits. These are the modern analogues of many ancient ophiolite-hosted deposits[1–4], such as those exposed in Cyprus. Here we report results obtained from drilling a series of holes into an actively forming sulphide deposit on the Mid-Atlantic Ridge. A complex assemblage of sulphide–anhydrite–silica breccias provides striking evidence that such hydrothermal mounds do not grow simply by the accumulation of sulphides on the sea floor. Indeed, the deposit grows largely as an *in situ* breccia pile, as successive episodes of hydrothermal activity each form new hydrothermal precipitates and cement earlier deposits. During inactive periods, the collapse of sulphide chimneys, dissolution of anhydrite, and disruption by faulting cause brecciation of the deposit. The abundance of anhydrite beneath the present region of focused hydrothermal venting reflects the high temperatures (> 150 °C) currently maintained within the mound, and implies substantial entrainment of cold sea water into the interior of the deposit. These observations demonstrate the important role of anhydrite in the growth of massive sulphide deposits, despite its absence in those preserved on land.

In September–November 1994, the Ocean Drilling Program Leg 158 drilled a series of holes into a large hydrothermally active mound in the TAG hydrothermal field located at a water depth of 3,650 m on the eastern side of the median valley of the Mid-Atlantic Ridge at 26° 08′ N (Fig. 1 inset). Although hydrothermal deposits have been found over an area of about 5 × 5 km, known high-temperature venting is at present confined to the TAG active mound which is about 200 m in diameter and 50 m high[5–7]. Episodic hydrothermal activity at this site over at least the past 20,000 years[8,9] has resulted in the construction of two superposed platforms[10]. Mineralogical zoning on the surface of the mound reflects different, but related, types of venting (Fig. 1)[11,12]. Chalcopyrite–anhydrite-rich chimneys venting high-

[1]Department of Geology and Geophysics, Woods Hole Oceanographic Institution, Woods Hole, Massachusetts 02543, USA; [2]Institut fur Mineralogie, Tu Bergakademie Freiberg, 09595 Frieberg, Germany; [3]Ocean Drilling Program, Texas A&M University, College Station, Texas 77845, USA; [4]Department of Geological Sciences, University of Michigan, Ann. Arbor, Michigan 48109, USA; [5]Department of Marine Geology and Geophysics, Rosenstiel School of Marine and Atmospheric Sciences, University of Miami, Miami, Florida 33149, USA; [6]Institueo de Cicencias de la Tierra, CSIC, Marti i Franques s/n 08028, Barcelona, Spain; [7]Max-Planck Institut fur Chemie, Abteilung Geochemie, Postfach 3060, D-55020 Mainz, Germany; [8]Department of Earth and Planetary Sciences, Kyushu University 33, 6-10-1 Hakozaki, Fukuoka 812, Japan; [9]IFREMER Centre de Brest, DRO/GM, BP 70 29280 Plouzane, France; [10]CODES, University of Tasmania, GPO Box 252C, Hobart, Tasmania 7001, Australia; [11]Lamont-Doherty Earth Observatory, Palisades, New York 10964, USA; [12]Geological Survey of Canada, 601 Booth Street, Ottawa, Ontario K1A 0E8, Canada; [13]Department of Geology and Geochemistry, Stockholm University, S-10691, Stockholm, Sweden; [14]Institut de Geologie, Université Louis Pasteur, 1 rue Blessig, 67084 Strasbourg Cedex, France; [15]Department of Earth Sciences, University of Wales, Cardiff CF1 3YE, UK; [16]SOEST, University of Hawaii at Manoa, 2525 Correa Road, Honolulu, Hawaii 96822, USA; [17]Geological Survey of Japan, 1-1-3 Higashi, Tsukuba, Ibaraki 305, Japan; [18]Department of Biology, Indiana University, Bloomington, Indiana 47405, USA; [19]Institue of Marine and Coastal Sciences, Rutgers University, PO Box 231, New Brunswick, New Jersey 08903, USA; [20]Department of Geosciences, University of Houston, 4800 Calhoun, Houston, Texas 77204, USA; [21]Marine and Environmental Studies Program, University of San Diego, Camino Hall 8C, Alcala Park, San Diego, California 92110, USA; [22]Department of Marine Chemistry & Geochemistry, Woods Hole Oceanographic Institution, Woods Hole, Massachusetts 02543, USA; [23]Institute of Tectonics, Department of Earth Sciences, University of California, Santa Cruz, California 95064, USA.

temperature (>360 °C) copper-rich fluids are clustered on a 20 m diameter cone on the northwestern side of the upper platform (the Black Smoker complex). Approximately 70 m to the southeast on the lower platform, a field (the Kremlin area) of sphalerite-dominated, white smokers vent zinc-rich fluids at temperatures of 260–300 °C (refs 13–15). Geochemical modelling of fluid compositions and the associated mineral assemblages indicates that the white-smoker fluids can be derived from the black-smoker fluids by a combination of conductive cooling and mixing with sea water, and precipitation of sulphides and anhydrite within the mound[12,15]. These reactions decrease the pH of the circulating hydrothermal fluids to values below 3, causing dissolution of sphalerite within the mound and an order of magnitude enrichment of zinc in the white-smoker fluids (Zn concentration, 300–400 μmol l^{-1}) compared with the black-smoker fluids (Zn concentration, 46 μmol l^{-1})[15]. The zinc is then reprecipitated at the surface of the mound as sphalerite-rich chimneys and domes. Diffuse flow of low-temperature (<25 °C) fluids occurs over the rest of the top and sides of the mound.

Seventeen holes drilled at five locations (TAG 1–5) on the TAG active mound reveal the subsurface nature and lateral heterogeneity of the actively forming deposit and the underlying upflow zone down to the depth of 125 metres below sea floor (m.b.s.f.) (Fig. 1). Because holes were drilled in close proximity (within 10–15 m) at each location, their stratigraphy has been combined to produce a composite section for each area (Fig. 2). Recovery of relatively unaltered basalt near the edges of the mound at depths of about 20 m.b.s.f. (at TAG-2) and 40 m.b.s.f. (at TAG-4) has constrained the lateral extent of intense crustal alteration and mineralized upflow zone to about 80 m. Based on the thickness of the sulphide zone and the extent of the underlying upflow zone, our preliminary estimates indicate that there are about 2.7 million tonnes of massive sulphides above the sea floor, and approximately 1.2 million tonnes below the sea floor in the upflow zone. This is well within the range for typical ophiolite-based massive sulphide deposits worldwide[16] and is quite comparable with the average-sized Cyprus-type ore deposit of 3 million tonnes[17]. Shipboard analyses of samples from the drill core indicate bulk copper contents of 1–2 wt% for the deposit and imply a bulk metal content of 30–60 thousand tonnes of copper.

Breccias of various types dominate all the sections drilled through the mound (Fig. 2). Massive sulphides reflecting the formation of new hydrothermal precipitates (for example, massive granular pyrite and chalcopyrite at TAG-1, and massive sphalerite and pyrite at TAG-2) are restricted to the upper few metres at each drilling location. The near-surface precipitates at TAG-2 are relatively enriched in base metals (Zn contents of 1–4 wt%, Au contents of 3 p.p.m. compared with <700 p.p.m. and ~250 p.p.b. respectively at TAG-1); this is interpreted to be the result of remobilization of these metals at depth within the mound from previously deposited sulphides. Red and grey siliceous material (Fig. 3*a*) was also encountered in the upper few metres of the TAG-2, TAG-3 and TAG-4 areas. This probably results from the precipitation of silica at low temperatures (<100 °C) from hydrothermal fluids percolating through the mound.

Based on the overall internal structure of the mound and the upflow zone, four major zones can be distinguished, all of which may or may not be present in one section (Fig. 2). Zone 1 consists of clast-supported massive pyrite breccias that dominate the upper 10–20 m at every location (Fig. 3*b*). This is underlain by an anhydrite-rich zone (zone 2) identified only in the TAG-1 and TAG-5 areas. This zone can be divided into two breccia types distinguished primarily on the basis of the relative abundances of pyrite, anhydrite and silica: (1) matrix-supported pyrite–anhydrite breccias (Fig. 3*c*) are present down to about 30 m.b.s.f., and are underlain by (2) pyrite–silica–anhydrite breccias that extend to the bottom of the anhydrite-rich zone at about 45 m.b.s.f. Anhydrite veining is extremely well developed throughout this zone, where composite veins up to 45 cm thick are present (Fig. 3*d*). They comprise complex multi-stage fracture fillings and cavity linings, some of which include disseminated, fine-grained pyrite and chalcopyrite, and trace amounts of haematite. Zone 3 consists of intensely silicified and brecciated wall rock which comprises the upper portion of the upflow zone beneath the mound. Pyrite–silica breccias (Fig. 3*e*) occur in the upper part of this zone and are uderlain by silicified wall-rock breccias, which are distinguished from the overlying pyrite–silica breccias in that they contain significantly less pyrite (<50 vol.%) and are dominantly clast-supported. Below about 100 m.b.s.f., the silicified wall-rock breccias grade into a chloritized basalt breccia (zone 4) where chloritized and weakly mineralized basalt

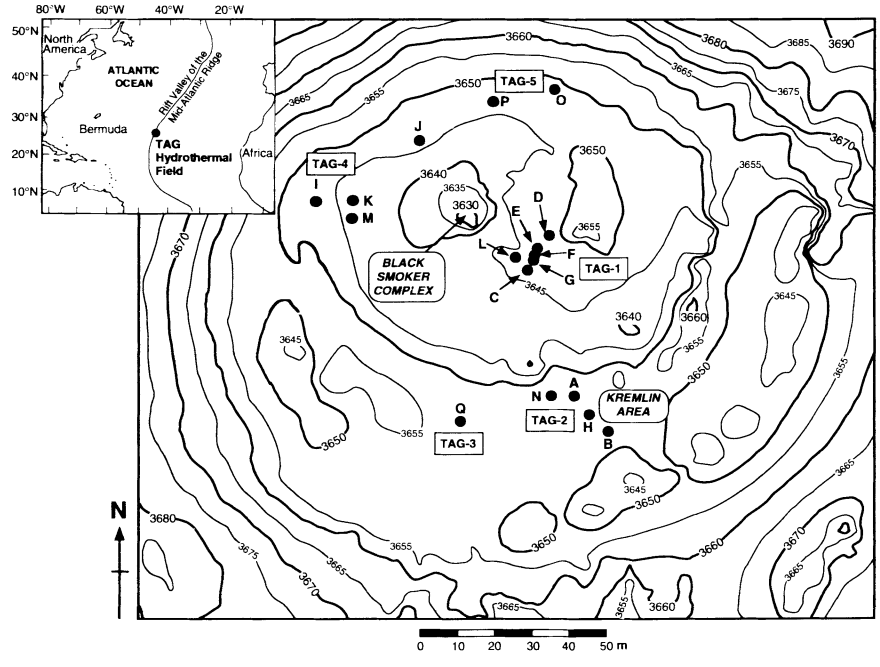

FIG. 1 High-resolution bathymetric map (5-m contour interval) of the TAG active mound, showing its overall morphology and the major areas of venting (Black Smoker complex and Kremlin area). The locations of the holes on the TAG active mound drilled during Leg 158 of the Ocean Drilling Program are also shown. Inset, location of the TAG hydrothermal field on the Mid-Atlantic Ridge. (Bathymetric map from M. C. Kleinrock and S.E.H., unpublished data).

fragments (1–5 cm in size) are cemented by quartz and pyrite, and are cross-cut by veins of pyrite, quartz and quartz + pyrite (Fig. 3*f*).

One of the most striking features of the cores recovered from the TAG mound is the dominance of breccias throughout the mound and in the upper parts of the underlying upflow zone. These breccias often include a mixture of clasts of various types (for example, sulphide, altered (silicified) wall rock) that formed by different processes at different depths. Of particular note is the presence of altered basalt fragments at shallow levels within the hydrothermal mound. This complex structure implies that the TAG active mound has undergone multiple stages of development, which are reflected in the sequences of alteration and veining events that can be distinguished in both the sulphide breccias and in the silicified and chloritized basalt breccias. The sulphide breccias probably accumulated at the sea floor by the collapse of large sulphide chimneys, mass wasting, and by dissection of massive sulphides by repeated movement along faults. This debris has been overgrown by later generations of deposits and progressively cemented or replaced by quartz, sulphides and sulphates. Closing and reopening of faults due to tectonic events could explain the focusing of fluid flow at this site during episodic hydrothermal activity. The presence of altered basalt clasts in the upper part of the mound may indicate (1) very high fluid flow rates[18] that transport the clasts from depth and then redeposit them at shallower depths, (2) emplacement of the sulphides within a pre-existing pillow mound or breccia pile which has now been largely replaced leaving behind relics of the original pillow talus, (3) partial burial of the deposit by lava flows at intermediate stages during its growth, or (4) disruption of the breccias and footwall rocks by faulting within the mound. The construction of the TAG active mound therefore is interpreted to be substantially a process of hydrothermal replacement and mineralization in the upflow zone coupled with mass wasting, brecciation and cementation of material that was precipitated on the sea floor.

The abundance of anhydrite preserved within the mound (estimated to be $\sim 10^5$ m^3) was unexpected. Owing to its retrograde solubility (that is, its solubility decreases with increasing temperature), the precipitation of anhydrite from sea water at a water depth of 3,650 m requires the sea water to be heated to >150 °C. Hence the presence of anhydrite reflects the high temperatures maintained within the mound, and its abundance implies substantial entrainment of cold sea water into the interior of the deposit. Estimates[5] of the convective heat flux from the Black Smoker complex are in excess of 200 MW. The focusing of this flux in a small area suggests that the vigorous high-velocity discharge of hot, hydrothermal fluids results in sea water being drawn into the edges of the mound and into the upflow zone beneath the Black Smoker complex[12] where it is heated by mixing with the high-temperature hydrothermal fluids. By this mechanism, many cubic kilometres of sea water may have been entrained over the life of the hydrothermal system. During long periods of inactivity, temperatures within the mound undoubtedly decreased below 150 °C causing abundant dissolution of anhydrite and resulting in the formation of open spaces and collapse breccias.

The internal structure of the TAG mound bears a striking resemblance to ancient volcanic-hosted massive sulphide deposits preserved in ophiolites. Such deposits found in the ophiolites of Cyprus, Oman and Newfoundland are regarded as the closest ancient analogues of massive deposits currently forming at mid-ocean ridges. Sulphide and wall-rock breccias are well documented in Cyprus-type massive sulphides and include coarse sulphide conglomerates, quartz-cemented breccias, and chloritized and silicified basalt breccias[16,19,20,21]. Metal-enriched zones similar to those in the upper few metres of the TAG active mound have been observed close to the palaeo sulphide–seawater inter-

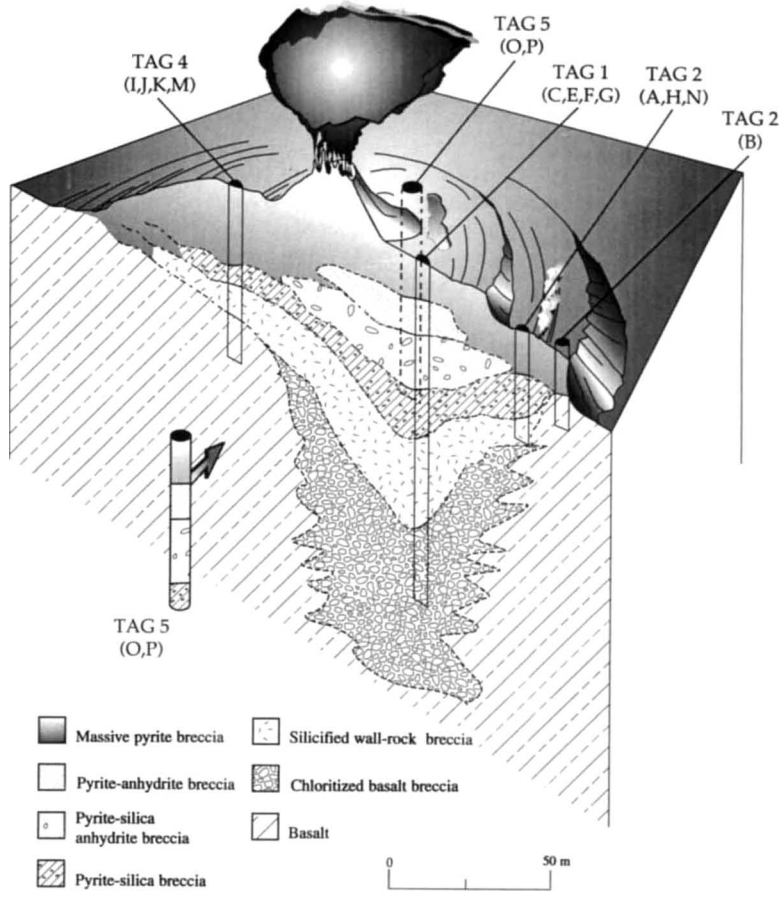

FIG. 2 Diagram of the TAG active mound showing the surface morphology and distribution of venting, as well as the generalized and simplified internal structure based on the drilling results. Letters in brackets refer to the drillhole designations at each site, as shown in Fig. 1. Recovery of rock core ranged from <1 to 63% with an average of ~12%. Four major zones within the mound and upflow zone can be distinguished. Zone 1. Massive pyrite breccias—clasts (up to 5 cm) of massive, granular pyrite in a porous, sandy pyrite matrix with minor amounts of anhydrite (Fig. 3*b*). Pyrite typically comprises >75 vol.% of the rock. Zone 2. Pyrite–anhydrite breccias down to about 30 m.b.s.f.—rounded pyrite clasts (0.5–2 cm in size) in a matrix of anhydrite (Fig. 3*c*). Pyrite comprises 50–75 vol.%, anhydrite >25 vol.%. Pyrite–silica–anhydrite breccias that extend to ~45 m.b.s.f.—clasts of siliceous pyritic material, quartz–pyrite aggregates, and granular pyrite cemented mainly by quartz with cross-cutting anhydrite veins. Pyrite comprises 50–75 vol.%, silica >10 vol.%, and anhydrite >10 vol.%. Anhydrite veining is extremely well developed throughout this zone (Fig. 3*d*). Zone 3. Pyrite–silica breccias—large (≤10 cm) grey fragments of siliceous material (pre-existing mineralized and silicified wall rock) and quartz–pyrite clasts in a matrix of fine-grained quartz (Fig. 3*e*). Pyrite comprises >50 vol.%, quartz matrix >10 vol.%. Silicified wall-rock breccias—clasts of basaltic fragments (1–5 cm in size) that are recrystallized to quartz, pyrite and a phyllosilicate, although some contain relict igneous textures. Zone 4. Chloritized basalt breccias occur below ~100 m—chloritized and weakly mineralized basalt fragments (1–5 cm in size) cemented by quartz and pyrite, and cross-cut by veins of pyrite, quartz and quartz + pyrite (Fig. 3*f*). (This figure was drawn by E. P. Oberlander.)

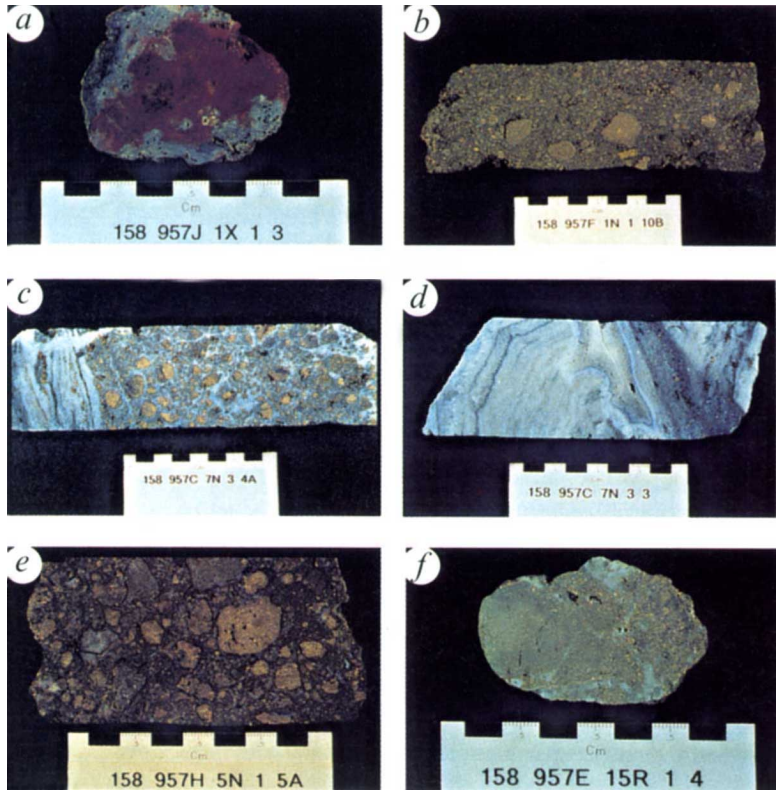

FIG. 3 Examples of different rock types comprising the subsurface portion of the TAG active hydrothermal mound. Scale bar in each photograph is divided in 1 cm intervals. *a*, Red and grey siliceous material (sample 158-957J-1X-1, piece 3) from 0.2 m.b.s.f. from the TAG-4 area. It consists of massive iron oxide bearing silica (red colouration) surrounded by grey quartz and chalcedony. The contacts between red and grey siliceous zones are irregular, sharp or gradational. Pyrite is rare in the red silica, but occurs as fine-grained, disseminated euhedral grains and as colloform layers in the grey silica. *b*, Pyrite breccia (sample 158-957F-1N-1, piece 10B from 1.4 m.b.s.f. from the TAG-1 area) composed of clasts of massive granular pyrite in a porous, sandy pyrite matrix with minor anhydrite (<10 vol.%). An angular chalcopyrite clast, similar in texture to the innermost, monomineralic chalcopyrite lining the black-smoker chimneys[12] is present. *c*, Pyrite–anhydrite breccia (sample 158-957C-7N-3, piece 4A from 23 m.b.s.f. from the TAG-1 area) is the principal sulphide type in the anhydrite-rich zone. It consists of rounded clasts of massive granular pyrite in a matrix of massive to semimassive anhydrite with minor disseminated sulphides. With increasing depth, siliceous clasts and quartz–pyrite clasts become increasingly common as this rock type grades into a siliceous pyrite–anhydrite breccia. The contact with the overlying zone of anhydrite veins (which is at least 30 cm thick) can be seen. This portion of the vein contains at least two, and possibly three, generations of anhydrite veins. *d*, Portion of the same anhydrite vein (sample 158-957C-7N-3, piece 3) shown in *c* and oriented in the same direction. It consists of massive granular banded anhydrite with fine, disseminated pyrite and/or chalcopyrite along the growth bands. The 2-cm-wide, dark-grey band comprises a second vein type that occurs locally within the large anhydrite vein. It is composed of coarsely crystalline anhydrite with abundant, uniformly disseminated pyrite and chalcopyrite. Late coarse-grained, barren anhydrite replaces earlier massive banded anhydrite as concentric zones around a late fracture. *e*, Pyrite–silica breccia (sample 158-957H-5N-1 piece 5A from 27 m.b.s.f. from the TAG-2 area) composed of rounded clasts of pyrite in a matrix of very fine-grained quartz. Clasts of siliceous wall rock (consisting of grey-to-white quartz plus variable amounts of pyrite) are also present. *f*, Chloritized basalt breccia (sample 158-957E-14R-1, piece 10 from 102 m.b.s.f. from the TAG-1 area) consisting of grey basaltic fragments pervasively altered to chlorite, a clay mineral (perhaps sericite), and/or quartz in a matrix of dark-grey quartz and pyrite. Pyrite occurs as 1–4 mm wide zones and chalcopyrite occurs as rims, on the margins of altered basaltic clasts. Veins of pyrite, quartz and pyrite + quartz cross-cut the basaltic fragments.

face in volcanogenic massive sulphide deposits on land, and the siliceous material is analogous to the red cherts (jasper) associated with many of the Cyprus-type deposits[16]. The abundance of breccia ores and sulphide conglomerates in the Cyprus deposits was previously explained as post-depositional weathering and destruction of the mounds[20,22]. The observations at TAG suggest, however, that these breccias were probably formed at the time of high-temperature venting and were initially cemented by anhydrite. Anhydrite is now absent from the Cyprus deposits because it dissolved soon after high-temperature hydrothermal activity had ceased. Although the complex assemblage of breccias partly confirms models of deposit growth deduced from the study of Cyprus-type deposits, the importance of anhydrite in this process had not been predicted, and would not have been revealed without drilling an active sea-floor massive sulphide deposit. □

Received 9 June; accepted 16 September 1995.

1. Spooner, E. T. C. in *Deep Drilling Results in the Atlantic Ocean: Ocean Crust* (eds Talwani, M., Harrison, C. G. & Hayes, D. E.) 429–431 (Am. Geophys. Un., Washington DC., 1978).
2. Spooner, E. T. C. *Geol. Ass. Canada Spec. Pap.* **20,** 685–704 (1980).
3. Rona, P. A. & Scott, S. D. *Econ. Geol.* **88,** 1935–1975 (1993).
4. Herzig, P. M. & Hannington, M. D. *Ore Geol. Rev.* (in the press).
5. Rona, P. A. *et al. Econ. Geol.* **18,** 1989–2017 (1993).
6. Rona, P. A. *et al. J. geophys. Res.* **98,** 9715–9730 (1993).
7. Rona, P. A., Klinkhammer, G., Nelsen, T. A., Trefry, J. H. & Elderfield, H. *Nature* **321,** 33–37 (1986).
8. Lalou, C. *et al. Earth planet. Sci. Lett.* **97,** 113–128 (1990).
9. Lalou, C. *et al. J. geophys. Res.* **98,** 9705–9713 (1993).
10. Humphris, S. E., Kleinrock, M. C. & Deep-TAG Team (abstr.) *Eos* **75,** 660 (1994).
11. Thompson, G., Humphris, S. E., Schroeder, B., Sulanowska, M. & Rona, P. A. *Can. Mineralogist* **26,** 697–711 (1988).
12. Tivey, M. K., Humphris, S. E., Thompson, G., Hannington, M. D. & Rona, P. A. *J. geophys. Res.* **100,** 12527–12555 (1995).
13. Campbell, A. C. *et al. Nature* **335,** 514–519 (1988).
14. Edmond, J. M., Campbell, A. C., Palmer, M. R. & German, C. R. (abstr.) *Eos* **71,** 1650–1651 (1990).
15. Edmond, J. M. *et al.* in *Hydrothermal Vents and Processes* (eds Parson, L. M., Walker, C. L. & Dixon, D. R.) 77–86 (Geol. Soc. Spec. Publ., London, 1995).
16. Franklin, J. M., Lydon, J. W. & Sangster, D. F. *Econ. Geol.* **75,** 485–627 (1981).
17. Strens, M. R. & Cann, J. R. *Tectonophysics* **122,** 307–324 (1986).
18. Strens, M. R. & Cann, J. R. *Geophys. J. R. astr. Soc.* **71,** 225–240 (1982).
19. Adamides, N. G. thesis, Univ. Leicester (1984).
20. Constantinou, G. in *Proc. Int. Ophiolite Symp. on Ophiolites* (ed. Panayioutou, A.) 663–674 (Cyprus Geol. Surv. Dept., Nicosia, 1980).
21. Lydon, J. W. *Geol. Surv. Can. Pap.* **84-1A,** 601–610 (1984).
22. Constantinou, G. *Geol. Ass. Can. Spec. Pap.* **14,** 187–210 (1976).

ACKNOWLEDGEMENTS. We wish to express our gratitude to the drilling, ship and scientific staff on board the D/V *JOIDES Resolution* for their help during ODP Leg 158.